An Imidazolate-Bridged Tetranuclear Copper(II) Complex: Synthesis, Magnetic and EPR Studies, and Crystal Structure of $[L_4Cu_4(Im)_4](ClO_4)_4 \cdot 2H_2O$ (L = 1,4,7-Triazacyclononane, Im = Imidazolate Anion)

Phalguni Chaudhuri,*,† Ina Karpenstein,† Manuela Winter,† Marek Lengen,‡ Christian Butzlaff,‡ Eckhard Bill,‡ Alfred X. Trautwein,*,‡ Ulrich Flörke,§ and Hans-Jürgen Haupt§

Anorganische Chemie I, Ruhr-Universität, W-4630 Bochum, Germany, Institut für Physik, Medizinische Universität, W-2400 Lübeck, Germany, Allgemeine Anorganische und Analytische Chemie, Universität-Gesamthochschule Paderborn, W-4790 Paderborn, Germany

Received June 5, 1992

The tetranuclear complex $[L_4Cu_4(Im)_4](ClO_4)_4 \cdot 2H_2O$, where L is the cyclic amine 1,4,7-triazacyclononane and Im^- is the imidazolate anion, has been synthesized and its structure determined by X-ray diffraction methods as having imidazolate as bridging ligands. The complex crystallizes in monoclinic space group $P2_1/c$ with cell constants a = 15.088(4) Å, b = 14.430(3) Å, c = 14.713(5) Å, β = 102.05(2)°, V = 313.73(1.52) Å^3, and Z = 2. Each of the four LCu units is coordinated via two imidazolate anions (Im^-) to two LCu units, yielding four distorted square pyramidal CuN_5 polyhedra. The four copper ions which lie on a plane form an approximate parallelogram with sides of 5.89 and 5.99 Å. The compound has also been studied with variable temperature (2–295 K) magnetic susceptibility measurements and X-band EPR spectroscopy. Analysis of the susceptibility data yields an antiferromagnetic interaction between adjacent Cu(II) centers. The following parameter values are obtained: J = 70 cm^{-1}, g = 2.16, $[\hat{H} = J(\vec{S}_1 \cdot \vec{S}_2 + \vec{S}_2 \cdot \vec{S}_3 + \vec{S}_3 \cdot \vec{S}_4 + \vec{S}_1 \cdot \vec{S}_4]$. The electronic state has been established to have $S_t = 0$. The X-band EPR spectra, recorded in the temperature range 2.7–295 K are governed by an isotropic, almost temperature independent resonance C1 at g = 2.10. A second component C2, which arises above 20 K, exhibits significant temperature dependence with maximum at about 40 K. A satisfactory simulation of the subspectrum C2 has been obtained using the following parameters: isotropic g_{111} = 2.1, and zero-field values D_{111} = 0.23 cm^{-1} and $E/D_{111} \approx 0.06$. The EPR subspectra C1 and C2 have been assigned to the highest quintet $|112\rangle$ and to the first excited triplet state $|111\rangle$ of the tetramer, respectively.

Introduction

Imidazole (ImH), a five-membered nitrogen heterocycle, is an ubiquitous ligand in chemical and biological systems. It occurs in proteins as part of the side chain of the amino acid histidine,[1] in nucleic acid structures as part of the purine ring of adenine and guanine,[2] and in the vitamin B_{12} coenzyme as benzimidazole.[3] In these systems the imidazole functions in a variety of roles: for example, as a proton donor and/or acceptor site for hydrogen bonding, as a specific/general base or nucleophilic catalyst, or as a site of metal ion coordination.[4] The imidazole moiety of histidyl residues in a large number of metalloproteins constitutes all or part of the binding sites of various transition metal ions such as Mn^{2+}, $Fe^{2+/3+}$, $Cu^{+,2+}$, and Zn^{2+}. As for example, its conjugate base, the imidazolate ion (Im^-), is known to act as a bridging ligand between copper(II) and zinc(II) in bovine erythrocyte superoxide dismutase (BESOD).[5] Thus, structural and spectroscopic studies that characterize the bonding between imidazole and transition-metal ions are of considerable importance.

The impetus for the synthesis of trinuclear and/or tetranuclear copper clusters and the study of their physical and chemical properties is the recent unambiguous demonstration of the existence of a 3 + 1 arrangement of the copper atoms in the structure of the oxidized ascorbate oxidase[7] from courgettes. Fascinating examples of copper(II) clusters with various nuclearities have been described in the literature.[8] The potential for different cluster formation by Cu(II) ions suggests new synthetic targets and reinforces the point that many new structures remain to be discovered as synthetic molecules or as active sites in proteins. Such complexes are currently of interest from the magneto-structural and biomodeling points of view. Unfortunately only a few of the structurally characterized compounds have been the subject of a combined EPR and magnetic susceptibility investigation.[6]

For some time we have been interested in low-molecular weight copper-containing complexes, which may serve as structural and spectroscopic models for the active sites of copper metalloproteins.[9] Recently we have prepared and examined an imidazolate-bridged tricopper complex[10] as a first generation model for the active site of ascorbate oxidase. As a part of our continuous efforts to prepare copper complexes with variable multiatom bridging ligands,[11] we

† Universität Bochum.
‡ Medizinische Universität zu Lübeck.
§ Universität-Gesamthochschule Paderborn.

(1) Creighton, T. E. *Proteins, Structures and Molecular Properties*; W. H. Freeman: New York, 1984.
(2) Saenger, W. *Principles of Nuclei Acid Structure*; Springer-Verlag: New York, 1984.
(3) Pratt, J. M. *Inorganic Chemistry of Vitamin B_{12}*; Academic Press: New York, 1972.
(4) (a) Freeman, H. C. In *Inorganic Biochemistry*; Eichhorn, G. L., Ed.; Elsevier: New York, 1973; Chapter 4, p 143. (b) Sundberg, R. J.; Martin, R. B. *Chem. Rev.* **1974**, *74*, 471. (c) Bioinorganic Chemistry – State of the Art. *J. Chem. Educ.* **1985**, *62*, 917–1001.
(5) Richardson, J. S.; Thomas, K. A.; Rubin, B. H.; Richardson, D. C. *Proc. Natl. Acad. Sci. U.S.A.* **1975**, *72*, 1349.
(6) E.g.: Bencini, A.; Gatteschi, D.; Zanchini, C.; Haasnoot, J. G.; Prins, R.; Reedijk, J. *J. Am. Chem. Soc.* **1987**, *109*, 2926.
(7) Messerschmidt, A.; Rossi, A.; Ladenstein, R.; Huber, R.; Bolognesi, M.; Gatti, G.; Marchesini, A.; Petruzelli, R.; Finazzi-Agro, A. *J. Mol. Biol.* **1989**, *206*, 513.
(8) Ardizzoia, G. A.; Angaroni, M. A.; Monica, G. L.; Cariati, F.; Moret, M.; Masciocchi, N. *J. Chem. Soc., Chem. Commun.* **1990**, 1021 and references therein.
(9) Chaudhuri, P.; Oder, K.; Wieghardt, K.; Nuber, B.; Weiss, J. *Inorg. Chem.* **1986**, *25*, 2818.
(10) Chaudhuri, P.; Karpenstein, I.; Winter, M.; Butzlaff, C.; Bill, E.; Trautwein, A. X.; Flörke, U.; Haupt, H.-J. *J. Chem. Soc., Chem. Commun.* **1992**, 321.

0020-1669/93/1332-0888$04.00/0

have studied the ternary system: Cu^{2+}, imidazole, and the small tridentate cyclic amine 1,4,7-triazacyclononane (L). The reaction took place in a counterintuitive fashion and led to the isolation of a tetranuclear copper complex with four μ-imidazolate bridging ligands, $[L_4Cu_4(Im)_4](ClO_4)_4$, which is the subject matter of this paper.

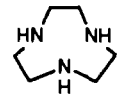

1,4,7,-Triazacyclononane

Imidazolate, Im

Imidazolate-bridged copper(II) complexes have been actively studied,[12-17] mainly to understand the factors determining the extent of coupling between the two metal ions and to use these simple compounds as models for metalloenzymes that contain the same structural units. Unfortunately, until now not much success has been achieved in finding useful correlations between structure and exchange coupling and more experiments appear to be required. We decided to collect magnetic data, together with EPR spectra, in order to characterize the magnetic coupling for this tetranuclear complex and hopefully to add a new brick to the construction of the correlation between structure and exchange coupling in imidazolate-bridged copper(II) complexes. In addition, there is a clear interest on trinuclear and tetranuclear metal complexes from the magnetochemists, because these complexes offer the opportunity to test magnetic exchange models (e.g. HDvV model) on more complicated systems than the extensively studied binuclear systems.[18]

Experimental Section

Materials and Methods. The macrocycle 1,4,7-triazacyclononane (L) was prepared as described in the literature.[19] All other starting materials were commercially available and were of reagent grade. Elemental microanalyses (C, H, N) were performed by the Microanalytical laboratory, Ruhr-Universität, Bochum, Germany. Copper was determined gravimetrically by using *N*-benzoyl-N-phenylhydroxylamine. The perchlorate anion was determined gravimetrically as tetraphenylarsonium-(V) perchlorate. Fourier transform infrared spectroscopy on KBr pellets was performed on a Perkin-Elmer 1720 X FT-IR instrument.

Magnetic susceptibilities of powdered samples were recorded on a SQUID magnetometer (MPMS, Quantum Design) in the temperature range 2–295 K with an applied field of 1 T. Experimental susceptibility data were corrected for the underlying diamagnetism.

The X-band EPR spectra of the polycrystalline material were recorded at various temperatures between 2.7 and 295 K with a Bruker ER 200 D-SRC spectrometer equipped with a standard TE 102 cavity, an Oxford Instruments liquid helium continuous-flow cryostat, a NMR gaussmeter, a frequency meter, and a data acquisition system (own development).

Preparation of the Compound $[(C_6H_{15}N_3)Cu(C_3H_3N_2)]_4(ClO_4)_4 \cdot 2H_2O$. To a suspension of $Cu(CH_3COO)_2 \cdot H_2O$ (0.4 g, 2 mmol) in methanol (30 mL) was added a solid sample of imidazole (0.14 g, 2 mmol), and the suspension was refluxed for 0.5 h to give a blue solution. A solution of the cyclic amine (0.26 g, 2 mmol) in 10 mL of methanol was added to the aforementioned blue solution and the resulting deep blue solution was filtered to get rid of any solid particles, followed by an addition of 0.6 g of $NaClO_4 \cdot H_2O$ to the filtrate. The solution kept at ambient temperature provided deep blue crystals. The crystals were collected by filtration and air-dried. Yield: 60–70%. Anal. Calcd for $CuC_9H_{18}N_5(ClO_4) \cdot 5H_2O$: C, 29.35; H, 5.20; N, 19.02; Cu, 17.25; ClO_4, 27.00. Found: C, 29,5; H, 5.20; N, 19.2; Cu 17.5; ClO_4 27.3. *Caution*: Although we experienced no difficulties with the perchlorate salt, the unpredictable behavior of perchlorate salts necessitates extreme caution in their handling.

Table I. Crystallographic Data for $[(C_6H_{15}N_3)(C_3H_3N_2)Cu]_4(ClO_4)_4 \cdot 2H_2O$

formula	$[C_{36}H_{72}N_{20}O_{16}Cl_4Cu_4] \cdot 2H_2O$	Z	2
		D_{calcd}, g cm^{-3}	1.562
fw	1473.1	$F(000)$	1520
space group	$P2_1/c$ (C_{2h}^5, No. 14)	R	0.097
		R_w	0.087
a, Å	15.088(4)	T, °C	23
b, Å	14.430(3)	λ(Mo Kα, graphite monochromated), Å	0.710 73
c, Å	14.713(5)		
β, deg	102.05(2)	μ, mm^{-1}	1.59
V, Å^3	3132.73(1.52)		

Crystal Structure Determination. A blue crystal of $[(C_6H_{15}N_3)_4(C_3H_3N_2)_4Cu_4](ClO_4)_4 \cdot 2H_2O$ with dimensions of 0.19 × 0.20 × 0.45 mm was mounted on a Siemens R3m/V diffractometer. Preliminary examinations showed that the crystal belonged to the monoclinic crystal system, space group $P2_1/c$. The lattice parameters were obtained at 23 °C by a least-squares refinement of the angular settings ($10° \leq 2\theta \leq 30°$) of 25 reflections. The data are summarized in Table I. The data were corrected for Lorentz and polarization effects, but it was not necessary to account for crystal decay. An empirical absorption correction[20] was carried out (ψ scans). The scattering factors[21] for neutral non-hydrogen atoms were corrected for both the real and the imaginary components of anomalous dispersion. The structure was determined by direct methods (SHELXTL-PLUS). The structure was refined by a least-squares technique; the function minimized was $\sum w(|F_o| - |F_c|)^2$ where $1/w = \sigma^2(F) + 0.001F^2$. Idealized positions of H atoms bound to carbon atoms were calculated (C–H = 0.96 Å) and included in the refinement cycle with a common isotropic thermal parameter (U_{iso} = 0.080 Å^2). All non-hydrogen atoms were refined anisotropically; oxygen atoms showed large displacement parameters indicating partial disorder of the perchlorate ions, which could not be resolved. Final positional parameters are presented in Table II, while selected interatomic distances and angles are given in Table III.

Results and Discussion

The pale blue solution containing bis(imidazole)copper(II) diacetate, $[Cu(ImH)_2(OAc)_2]$[22] reacts with the cyclic amine in methanol to afford, after addition of the perchlorate ion, deep blue tetranuclear complex $[(C_6H_{15}N_3)_4Cu_4(Im)_4](ClO_4)_4$ in good yields.

Description of the Structure. The molecular geometry and the atom-labeling scheme of the cation are shown in Figure 1. The structure of the complex molecule consists of a centrosymmetric tetranuclear cation $[(C_6H_{15}N_3)_4(Im)_4Cu_4]^{4+}$, four noncoordinatively bound perchlorate anions, and two water molecules. Each of the four $(C_6H_{15}N_3)Cu$ units is coordinated via two imidazolate anions (Im^-) to two $(C_6H_{15}N_3)Cu$ units, yielding four distorted square pyramidal CuN_5 polyhedra. The four copper ions which lie on a plane form an approximate parallelogram of sides 5.89 Å (Cu(1)···Cu(2)) and 5.99 Å (between Cu(1) and Cu(2a)). In the cation the angles Cu(2)–Cu(1)–Cu(2a) and Cu(1)–Cu(2)–Cu(1a) have been found to be 96.6 and 83.4°, respectively. The copper ion Cu(1) is coordinated to two nitrogen atoms N(5) and

(11) Chaudhuri, P.; Winter, M.; Della Védova, B. P. C.; Bill, E.; Trautwein, A. X.; Gehring, S.; Fleischhauer, P.; Nuber, B.; Weiss, J. *Inorg. Chem.* **1991**, *30*, 2148 and references therein.
(12) Kolks, G.; Lippard, S. J.; Waszczak, J.; Lilienthal, H. R. *J. Am. Chem. Soc.* **1982**, *104*, 717.
(13) Matsumoto, K.; Ooi, S.; Nakao, Y.; Mori, W.; Nakahara, A. *J. Chem. Soc., Dalton Trans.* **1981**, 2045.
(14) Coughlin, P. K.; Lippard, S. J. *Inorg. Chem.* **1984**, *23*, 1446.
(15) (a) Bencini, A.; Benelli, C.; Gatteschi, D.; Zanchini, C. *Inorg. Chem.* **1986**, *25*, 398. (b) Benelli, C.; Bunting, R. K.; Gatteschi, D.; Zanchini, C. *Inorg. Chem.* **1984**, *23*, 3074.
(16) Matsumoto, N.; Akui, T.; Murakami, H.; Kanesaka, J.; Ohyoshi, A.; Okawa, H. *J. Chem. Soc., Dalton Trans.* **1988**, 1021.
(17) Salata, C.; Youinou, M. T.; Burrows, C. J. *Inorg. Chem.* **1991**, *30*, 3454.
(18) (a) *Magneto-Structural Correlations in Exchange Coupled Systems*; Wilett, R. D.; Gatteschi, D.; Kahn, O.; Eds.: Reidel, Dordrecht, The Netherlands, 1985. (b) Hatfield, W. E. In *Theory and Applications of Molecular Paramagnetism*; Boudreaux, E. A., Mulay, L. N., Eds.: John Wiley & Sons: New York, 1976; p 350. (c) O'Connor, C. J. *Prog. Inorg. Chem.* **1982**, *29*, 203.
(19) (a) Richman, J. E.; Atkins, T. J. *J. Am. Chem. Soc.* **1974**, *96*, 2268. (b) Wieghardt, K.; Schmidt, W.; Nuber, B.; Weiss, J. *Chem. Ber.* **1979**, *112*, 2220.
(20) SHELXTL-PLUS Program package 3 by G. M. Sheldrick, Universität Göttingen, 1988. Computations were carried out on a Microwax II computer.
(21) *International Tables for X-ray Crystallography*; Kynoch: Birmingham, England 1974; vol. 4.
(22) Henriksson, H. A. *Acta Crystallogr.* **1977**, *B33*, 1947.

Table II. Atomic Coordinates ($\times 10^4$) and Equivalent Isotropic Displacement Coefficients ($Å^2 \times 10^3$) for $[C_9H_{18}N_5Cu]_4(ClO_4)_4 \cdot 2H_2O$

	x	y	z	U(eq)[a]
Cu(1)	-2180(1)	1490(1)	70(1)	43(1)
Cu(2)	1512(1)	1638(1)	2375(1)	43(1)
N(1)	-977(8)	2010(9)	588(9)	42(5)
N(2)	436(8)	2071(9)	1459(8)	40(5)
C(1)	-664(11)	2901(11)	575(11)	41(7)
C(2)	174(12)	2938(11)	1110(12)	51(8)
C(3)	-296(12)	1578(11)	1099(11)	48(7)
N(3)	-1740(9)	760(9)	-882(9)	44(6)
N(4)	-1441(9)	-367(8)	-1796(9)	49(6)
C(4)	-1300(11)	1119(11)	-1528(12)	51(8)
C(5)	-1135(10)	455(11)	-2087(12)	53(8)
C(6)	-1799(11)	-114(11)	-1061(11)	46(7)
N(5)	-2686(9)	2009(9)	1154(9)	50(6)
N(6)	-3028(8)	2644(9)	-660(9)	48(6)
N(7)	-3408(9)	806(9)	-196(10)	53(6)
C(7)	-2802(12)	3004(12)	1005(12)	65(9)
C(8)	-3356(11)	3182(11)	41(13)	66(9)
C(9)	-3695(11)	2135(14)	-1324(11)	64(8)
C(10)	-4094(11)	1332(13)	-818(13)	73(9)
C(11)	-3607(13)	652(13)	712(14)	79(10)
C(12)	-3502(12)	1525(14)	1270(12)	72(9)
N(8)	2692(10)	1323(10)	3294(11)	71(7)
N(9)	996(10)	1518(11)	3686(9)	69(7)
N(10)	1870(9)	2974(8)	2877(10)	51(6)
C(13)	2440(15)	752(12)	4003(15)	98(11)
C(14)	1684(15)	1197(14)	4436(13)	88(11)
C(15)	772(12)	2531(13)	3812(13)	78(10)
C(16)	1513(13)	3168(11)	3708(12)	66(9)
C(17)	2855(13)	2999(12)	3069(13)	73(10)
C(18)	3230(11)	2166(13)	3623(15)	88(10)
Cl(1)	1533(4)	5526(3)	1762(4)	70(2)
O(11)	1681(12)	5109(12)	2623(13)	158(7)
O(12)	2183(13)	5327(14)	1313(14)	179(8)
O(13)	690(10)	5274(10)	1213(11)	119(5)
O(14)	1543(8)	6522(10)	1922(9)	98(4)
Cl(2)	3909(4)	3230(4)	6152(4)	78(2)
O(21)	4482(15)	2541(17)	6361(17)	225(10)
O(22)	4101(13)	3870(15)	6856(15)	202(9)
O(23)	4081(10)	3684(11)	5366(11)	128(6)
O(24)	2987(8)	2910(8)	6026(8)	78(4)
Wa	4885(17)	4660(1)	1470(18)	298(13)

[a] Equivalent isotropic U defined as one-third of the trace of the orthogonalized U_{ij} tensor.

N(7), of the cyclic amine, two nitrogen atoms, N(1) and N(3), of the bridging imidazolate anions in the basal plane, and the third nitrogen atom, N(6), of the cyclic amine in the apical position. The four nitrogen atoms N(10), N(8), N(4a), and N(2) form the basal plane for the copper ion Cu(2). The average Cu–N(cyclic amine) and Cu–N(imidazolate) bond distances in the equatorial plane are 2.064 and 1.985 Å, respectively, and are considered as normal covalent bonds. The axial Cu–N(cyclic amine) bond is longer, 2.23 Å (average), as is expected for square pyramidal complexes of copper(II) and has been observed earlier.[11] The Cu–N(imidazolate) distance in this compound is slightly shorter than that of the imidazolate-bridged trinuclear complex[10] $[(C_9H_{21}N_3)_3Cu_3(Im)_3]^{3+}$ and falls within the reported range of 1.92–2.00 Å for other Cu–N(Im) bond lengths.[10,12-14,23,24] Selected bond distances and angles are listed in Table III.

The copper ion Cu(1) is displaced by 0.14 Å from the mean basal plane of four nitrogen atoms N(1), N(3), N(5), and N(7) toward the apical N(6) atom of the macrocyclic amine. The dihedral angles between the plane N(1)N(3)N(5)N(7) containing the Cu(1) ion and the planes N(3)C(4)N(4)C(5)C(6) and N(1)C(3)N(2)C(2)C(1) describing the two imidazolate bridging groups are 50.2 and 76.9°, respectively. The corresponding dihedral angles between the plane Cu(2)N(2)N(4a)N(8)N(10) and the

(23) Ivarsson, G.; Lundberg, B. K. S.; Ingri, N. *Acta Chem. Scand.* 1972, *26*, 3005.
(24) Lundberg, B. K. S. *Acta Chem. Scand.* **1972**, *26*, 3902.

Table III. Selected Bond Lengths (Å) and Angles (deg) for $[(C_6H_{15}N_3)_4Cu_4(Im)_4](ClO_4)_4 \cdot 2H_2O$ with Their Esd's in Parentheses

Cu(1)···Cu(2)	5.891(3)	Cu(1)–Cu(2)–Cu(1a)	83.4(5)
Cu(1)···Cu(2a)	5.987(3)	Cu(2)–Cu(1)–Cu(2a)	96.6(5)
Cu(1)–N(1)	1.965(12)	Cu(2)–N(2)	1.983(11)
Cu(1)–N(3)	1.975(14)	Cu(2)–N(4a)	2.015(12)
Cu(1)–N(7)	2.064(13)	Cu(2)–N(8)	2.049(14)
Cu(1)–N(5)	2.048(14)	Cu(2)–N(10)	2.094(12)
Cu(1)–N(6)	2.234(12)	Cu(2)–N(9)	2.233(15)
N(1)–C(1)	1.371(20)	N(3)–C(4)	1.369(23)
N(1)–C(3)	1.298(20)	N(3)–C(6)	1.288(20)
N(2)–C(2)	1.378(20)	N(4)–C(5)	1.374(21)
N(2)–C(3)	1.327(20)	N(4)–C(6)	1.356(23)
C(1)–C(2)	1.344(21)	C(4)–C(5)	1.320(24)
N(1)–Cu(1)–N(3)	93.4(5)	N(2)–Cu(2)–N(4a)	92.0(5)
N(1)–Cu(1)–N(5)	91.3(5)	N(2)–Cu(2)–N(10)	93.6(5)
N(1)–Cu(1)–N(6)	107.0(5)	N(2)–Cu(2)–N(9)	103.1(5)
N(3)–Cu(1)–N(5)	169.2(5)	N(4a)–Cu(2)–N(8)	92.3(5)
N(3)–Cu(1)–N(6)	107.5(5)	N(4a)–C(2)–N(10)	166.8(6)
N(5)–Cu(1)–N(6)	80.4(5)	N(4a)–Cu(2)–N(9)	107.3(6)
N(1)–Cu(1)–N(7)	167.5(6)	N(2)–Cu(2)–N(8)	173.7(6)
N(3)–Cu(1)–N(7)	91.8(6)	N(8)–Cu(2)–N(9)	79.9(6)
N(5)–Cu(1)–N(7)	81.8(6)	N(8)–Cu(2)–N(10)	81.2(5)
N(6)–Cu(1)–N(7)	82.2(5)	N(9)–Cu(2)–N(10)	83.0(6)
Cu(1)–N(1)–C(1)	130.2(10)	Cu(1)–N(1)–C(3)	126.6(11)
Cu(1)–N(3)–C(6)	130.4(12)	Cu(2)–N(2)–C(3)	126.7(11)
Cu(2a)–N(4)–C(6)	126.0(11)	Cu(2a)–N(4)–C(5)	130.6(12)
C(1)–N(1)–C(3)	130.0 (12)	C(4)–N(3)–C(6)	104.5(14)
C(2)–N(2)–C(3)	100.8(12)	C(5)–N(4)–C(6)	103.4(13)
N(1)–C(1)–C(2)	108.3(13)	N(3)–C(4)–C(5)	109.9(14)
N(2)–C(2)–C(1)	110.1(14)	N(4)–C(5)–C(4)	108.2(16)
N(1)–C(3)–N(2)	117.7(14)	N(3)–C(6)–N(4)	113.9(15)

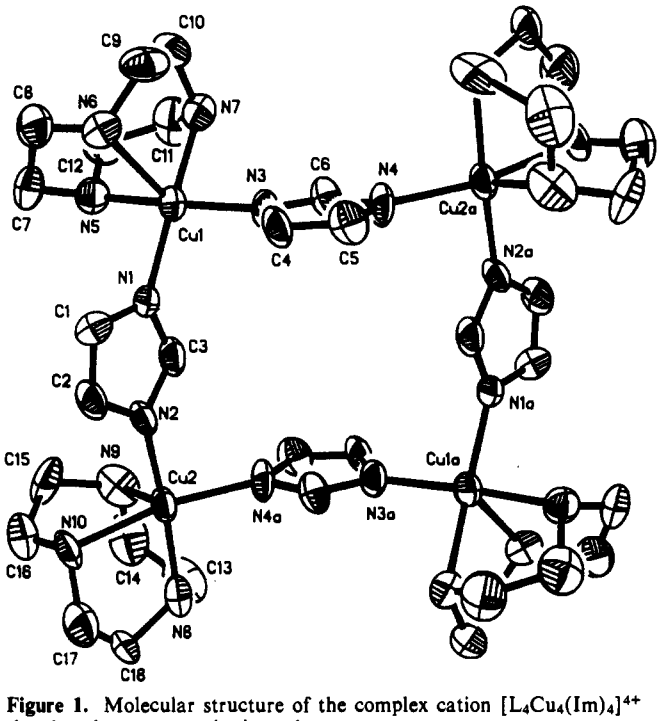

Figure 1. Molecular structure of the complex cation $[L_4Cu_4(Im)_4]^{4+}$ showing the atom-numbering scheme.

imidazolate ions are 95.7 and 26.9°, respectively. The dihedral angle between Cu(1)N(5)N(7)N(3)N(1) and Cu(2)N(2)N(4a)N(8)N(10) is 63.8°. It is interesting to note that the angle between the Cu(1)–N_{im}(1) and Cu(2)–N_{im}(2) vectors is 134.6°; the Cu(1)–N_{im}(3) vector makes an angle of 142.1° with the Cu(2a)–N_{im}(4) vector.

The bridging imidazolate rings are nearly planar, with the largest deviation from the mean plane being 0.01 Å. The imidazolate rings are flattened with the C(1)–N(1)–C(3), C(2)–N(2)–C(3), C(4)–N(3)–C(6), and C(5)–N(4)–C(6) angles

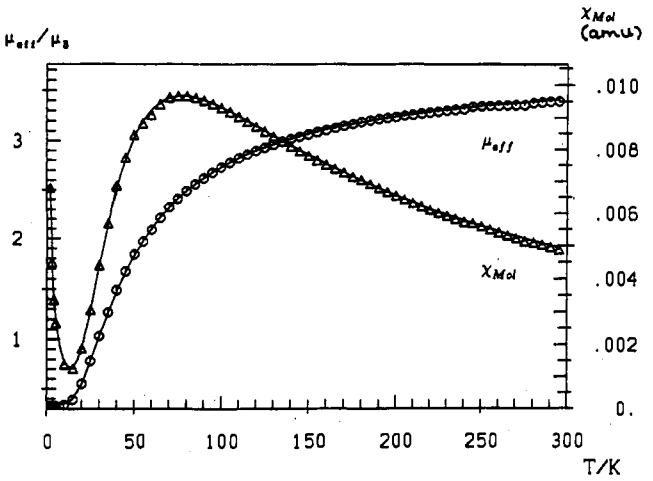

Figure 2. Molar magnetic susceptibility χ_{Mol} and effective magnetic moment μ_{eff} of the tetramer as a function of temperature. The solid lines represent the best least-squares fits of the experimental data on the basis of equation (eq 1) with $J = 70\ cm^{-1}$, $g = 2.16$, and an $S = {}^1/_2$ signal of 3.5% abundance.

smaller and the N(1)–C(3)–N(2) and N(3)–C(6)–N(4) angles larger than 108°. This type of flattening is typical for bridging imidazolate ligands.[13,14,25]

The largest deviation from idealized 90° interbond angles is 17°, which occurs within the angle N(Im)–Cu–N(amine), ranging between 91.3(5) and 107.5(5)°, whereas the N(amine)–Cu–N(amine) angles fall between 79.9(6) and 83.0(6)°. The C–N (average 1.459(23) Å) and C–C (average 1.517(27) Å) bond lengths between the methylene groups of the macrocyclic amine $C_6H_{15}N_3$ are unremarkable. The N–C (average 1.345(21) Å) and C–C (average 1.332(23) Å) bond lengths of the bridging imidazolate anions are found to be very similar to those observed in other comparable structures.

Magnetic Susceptibility. Magnetic susceptibility data for a polycrystalline sample of the tetranuclear complex were collected in the temperature range 2–295 K, and the temperature dependences of molar magnetic susceptibility χ_{Mol} and of effective magnetic moment μ_{eff} of the complex are displayed in Figure 2. The shapes of both plots reveal a behavior typical for antiferromagnetic spin coupling. The susceptibility plot exhibits the expected maximum between 74 and 79 K. Below 74 K χ_{Mol} decreases steadily until it reaches a minimum at 15 K. Below 15 K it starts again to increase. The magnetic moment decreases monotonically with decreasing temperature; the values of μ_{eff}/complex are 3.395 μ_B at 295 K, 2.727 μ_B at 100 K, 2.390 μ_B at 74 K, 0.388 μ_B at 15 K, and 0.330 μ_B at 2 K. Thus the magnetic data reveal an energetically well-isolated ground state of total spin $S_t = 0$, discernible from the decline of effective moments at temperatures below ≈100 K. The residual moment of 0.33 μ_B at 2 K and the corresponding rise of χ_{Mol} values below 15 K could be attributed to a monomeric ($S = {}^1/_2$) impurity (3.5%) (vide infra). Monomeric species appeared also in weak abundance in the EPR spectra, as will be mentioned below.

The susceptibility and EPR data could be simulated with a spin Hamiltonian assuming isotropic exchange interaction between adjacent Cu(II) pairs with local spins $S_i = {}^1/_2$, as sketched in Scheme Ia. Adopting the premise that all spin multiplets are well isolated and hence the total spin S_t is a good quantum number, we obtain the Hamiltonian

$$\hat{H} = g_t\mu_B\vec{B}\vec{S}_t + J(\vec{S}_1\cdot\vec{S}_2 + \vec{S}_2\cdot\vec{S}_3 + \vec{S}_3\cdot\vec{S}_4 + \vec{S}_1\cdot\vec{S}_4) = g_t\mu_B\vec{B}\vec{S}_t + J\vec{S}_A\cdot\vec{S}_B \quad (1)$$

(25) Haddad, M. S.; Duester, E. N.; Hendrickson, D. N. *Inorg. Chem.* **1979**, *18*, 141.

Scheme I. (a) Model of Spin Coupling in the Planar Tetramer and (b) Corresponding Spin States, Resulting from Eq 1 with $J > 0$ in Zero Applied Field

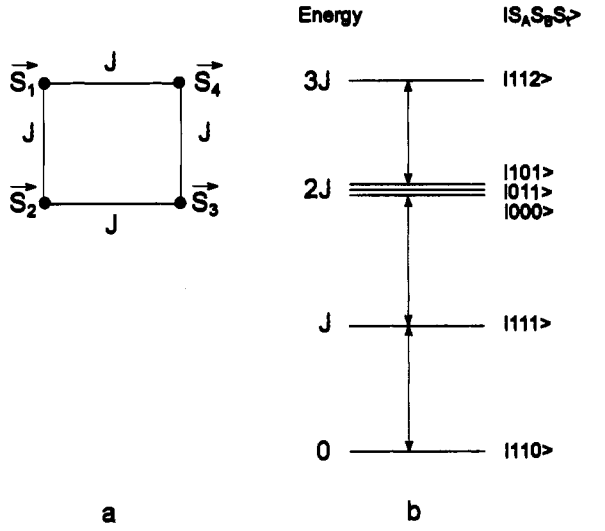

with $\vec{S}_t = \vec{S}_A + \vec{S}_B$, $\vec{S}_A = \vec{S}_1 + \vec{S}_3$, $\vec{S}_B = \vec{S}_2 + \vec{S}_4$, and $S_i = {}^1/_2$ for $i = 1, 2, 3, 4$.

Diagonalization of eq 1 with zero field yields spin multiplets as shown in Scheme Ib for antiparallel coupling. Note that we use the Heisenberg spin Hamiltonian in the form $\hat{H} = J\vec{S}_A\cdot\vec{S}_B$, with a positive J value corresponding to an antiferromagnetic interaction. The multiplets $|S_AS_BS_t\rangle$ are labeled by the "pair spins", S_A and S_B, and the total spin S_t. The ground state is a singlet $|110\rangle$, the first excited state at energy J is a triplet $|111\rangle$. The states $|011\rangle$ and $|101\rangle$ are degenerate at energy $2J$ and the highest state at energy $3J$ is a quintet $|112\rangle$. In zero field the multiplets remain degenerate in magnetic quantum numbers, according to their multiplicity. Projections of local spins S_i on the total spin S_t[26] reveal identical g_t values for all multiplets $S_t \neq 0$. The g values of the triplet $|111\rangle$ and of the quintet $|112\rangle$ are

$$g_{112} = g_{111} = (g_1 + g_2 + g_3 + g_4)/4 \quad (2)$$

and those of the triplets $|101\rangle$ and $|011\rangle$ are

$$g_{101} = (g_1 + g_3)/2 \quad g_{011} = (g_2 + g_4)/2 \quad (3)$$

As a result, g_t values in the coupled system are equal to the local g values of the Cu(II) ions, $g_t = g_i = g_{Cu}$.

The simulation of the experimental susceptibility data for the tetramer yielded an exchange coupling constant $J = 70\ cm^{-1}$ and $g_t = 2.16$, a value which is very similar to the value obtained from EPR, $g_t = 2.10$ (see below). The agreement between the calculated and observed magnetic data is very good, and the best fits using eq 1, with the $S = {}^1/_2$ impurities (3.5%) mentioned above, are shown as solid lines in Figure 2.

EPR Spectra. The X-band spectra of the tetramer, recorded in the temperature range 4.2–295 K, are governed by an isotropic, almost temperature independent resonance C1 at $g = 2.10$. Its line width appears to be almost constant ≈20–30 mT up to room temperature, while its intensity slightly increases at higher temperatures (Figure 3). Above 20 K, additional features of a second component C2 with wide splittings arise in the field range 80–400 mT. Its intensity exhibits significant temperature dependence with maximum at about 40 K (Figure 3). In the temperature range 20–295 K, which was relevant for the assignment of tetramer subspectra, neither of the two spectral components C1 and C2 could be power-saturated. Hence, it was not possible to unravel C1 and C2 by power-dependent measurements. For the following temperature-dependent analyses, we recorded spectra under nonsaturating conditions.

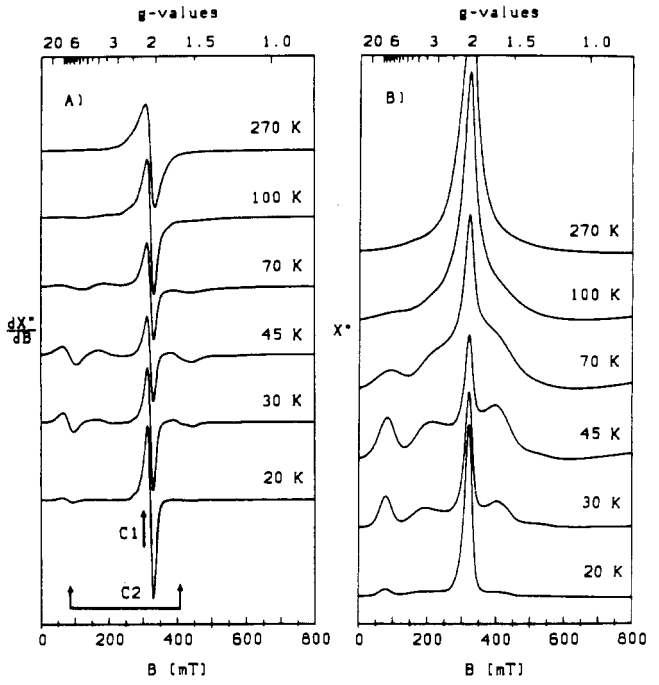

Figure 3. EPR spectra of a powder sample of $[L_4Cu_4(Im)_4](ClO_4)_4 \cdot 2H_2O$ recorded as a function of temperature in the range 20–270 K. (A) Experimental derivative spectra. Measuring conditions: microwave frequency, 9.437 GHz; power, 200 μW; modulation frequency, 100 kHz; modulation amplitude, 1 mT. The arrows mark the subspectra C1 and C2, mentioned in the text. (B) Absorption spectra derived from the spectra given in part A by numerical integration.

In order to elucidate the correlation between the EPR subspectra C1 and C2 and the spin multiplets of the coupled system, as presented in Scheme Ib, we analyzed the temperature dependence of the intensities I_{C1} and I_{C2}. To this end we first numerically integrated the experimental spectra. Then, we separated the isotropic absorption lines of C1 from the absorption pattern of C2 by linear interpolating the courses of C2 in the corresponding field range. Finally, the intensities I_{C1} and I_{C2} (spectral areas) were evaluated by independent integrations of the separated absorption curves. The separation of C1 and C2 is visualized as an example in Figure 5B. Subsequently, we plotted IT versus temperature T, which in first order is proportional to the Boltzmann function of the resonating levels.[30] In this presentation, an isolated spin manifold, obeying a Curie–Weiss law, would yield a horizontal straight line for $T \gg 0.4$ K. The subspectra C1 and C2 of the tetramer, however, exhibit a significant temperature dependence of $I_{C1}T$ and $I_{C2}T$, as shown in Figure 4A,B. The fading below 10 K and the strong rise at elevated temperatures prove that both subspectra C1 and C2 originate from excited states and that the ground state is diamagnetic and EPR silent, in accordance with the susceptibility findings. For temperatures above 100 K the evaluation of I_{C2} were obscured by large uncertainities due to fading of the derivative signals of C2. We observed increasing line broadening of C2 already above 70 K, which we relate to the onset of spin–lattice relaxation.

For quantitative analysis we compared the experimental data $I_{C2}T$ with theoretical Boltzmann functions, derived from the spin-coupling model (equation 1, Scheme I). Best agreement was obtained with the function $I_{111}T$ (Figure 4B), describing the thermal population of the first excited triplet state $|111\rangle$

$$I_{111}T \approx \exp(-J/kT)Z \tag{4}$$

$$Z = 1 + 3\exp(-J/kT) + 7\exp(-2J/kT) + 5\exp(-3J/kT) \tag{5}$$

The solid line in Figure 4B is a fit with $J = 78$ cm^{-1}, which is close

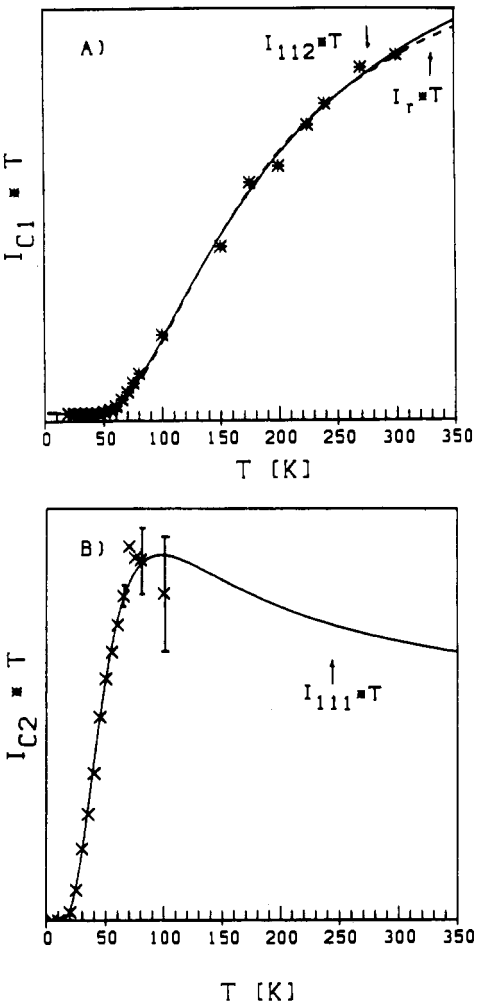

Figure 4. Temperature dependence of the temperature-weighted intensity of the EPR subspectra C1 (A) and C2 (B). Experimental conditions are as in Figure 3. The solid and dashed lines are calculated Boltzmann functions: (A) $I_{112}T$ (eq 7 with $J = 94$ cm^{-1}) and I_rT (eq 8 with $J = 132$ cm^{-1}); (B) $I_{111}T$ (eq 4 with $J = 78$ cm^{-1}).

to the exchange coupling constant $J = 70$ cm^{-1} evaluated from the susceptibility analysis. Hence, we assign the complex EPR spectrum of C2 to the first excited triplet state $|111\rangle$ of the tetramer.

The spread of resonances in the spectrum C2 (Figure 3, arrows) reveals that zero-field interaction is of the same order of magnitude as the Zeeman interaction (≈ 0.3 cm^{-1}). In order to quantitate these interactions we simulated subspectrum C2, using the usual effective spin Hamiltonian for spin $S = 1$:

$$\hat{H}_{111} = D_{111}[\tilde{S}_z^2 - {}^2/_3 + E/D_{111}(\tilde{S}_x^2 - \tilde{S}_y^2)] + g_{111}\mu\vec{B}\vec{S} \tag{6}$$

We found a satisfactory simulation of the C2 resonances of the 40 K EPR spectrum using as parameters the isotropic g value $g_{111} = 2.1$ and zero-field values $D_{111} = 0.23$ cm^{-1} and $E/D_{111} \approx 0.06$ (Figure 5A).

After having assigned subspectrum C2 to the $|111\rangle$ triplet state of the Cu tetramer, it is clear that subspectrum C1 must be related with one or several of the remaining multiplets $|101\rangle$, $|011\rangle$, or $|112\rangle$ (see Scheme Ib). However, unlike C2, C1 does not show a wide, complex resonance pattern, which is typical of an integer-spin system with zero-field interaction. The zero-field splittings, observed in the different spin manifolds of a Cu(II) tetramer originate from anisotropic (dipolar) component in the coupling of the individual Cu spins ($S_i = {}^1/_2$). If this anisotropy were significant, as shown here for one triplet, it should in principle affect all multiplets of the coupled system. Hence, also subspectrum C1 ought to represent this anisotropy. Under this aspect

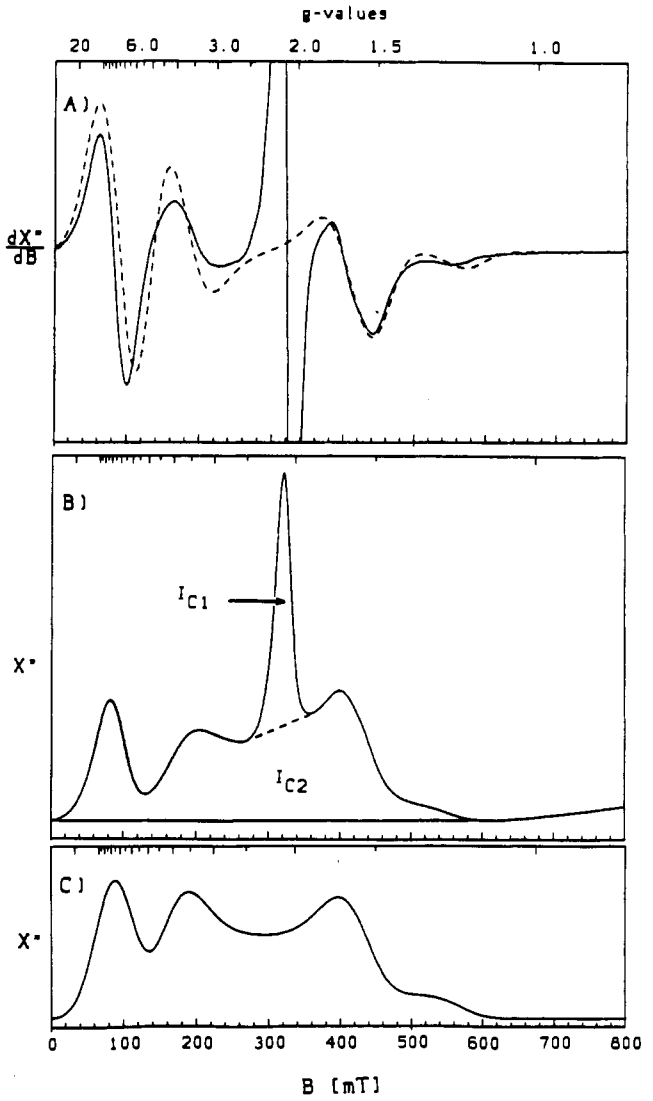

Figure 5. EPR spectrum of a powdered sample of $[L_4Cu_4(Im)_4](ClO_4)_4$ at 40 K. (A) Solid line: Experimental derivative spectrum (conditions as in Figure 3). Dashed line: Spin Hamiltonian simulation for a spin triplet S = 1, based on eq 6 with isotropic g value $g_{111} = 2.1$ and zero-field parameters $D_{111} = 0.23$ cm^{-1} and $E/D_{111} = 0.057$. The line shape was Gaussian with anisotropic line width (hwhm) $\Gamma_{x,y,z} = (31, 26, 33)$ mT. The positions of the different resonances in our simulation change by about only 20 mT if we take small variations of D_{111} (±0.005 cm^{-1}), E/D_{111} (±0.005), or g_{111} (±0.1). (B) Numerical integration of the experimental derivative spectrum, shown in part A. The dashed line visualizes the separation of the absorption pattern of C1 and C2, mentioned in the text. (C) Stimulated absorption spectrum (parameters as in part A).

it is surprising to observe a narrow and "isotropic" line. However, we assume that in our powder sample the spectral splitting of C1, which would be wide in a magnetically dilute system, collapses because exchange narrowing due to intermolecular spin–spin interaction of tetramers in the solid state.[26] Yet, it remains unclear why the narrowing effect is not observed for the triplet $|111\rangle$. A reason might be the higher spin multiplicity for the quintet, which could mediate stronger intermolecular spin–spin coupling, if the quintet would account for C1. We note that, on the other hand in a coupled system, any of the integer-spin multiplets might be EPR-silent, if the zero-field splitting of this manifold is sufficiently large to prevent EPR transitions between the magnetic substates.

The assignment of subspectrum C1 to a specified excited spin manifold is not unambiguous, if we consider the temperature variations of $I_{C1}T$. The experimental data can be described from a Boltzmann function $I_{112}T$ for the quintet $|112\rangle$ (Figure 4A, solid line), as well as with a function I_rT, which represents the combined contributions of all the remainig multiplets with $S_t \neq 0$ (Figure 4A, dashed line). The functions which we used were

$$I_{112}T \approx \exp(-3J/kT)/Z + \text{constant} \quad (7)$$

$$I_rT \approx (\exp(-2J/kT) + \exp(-3J/kT))/Z + \text{constant} \quad (8)$$

Both formulas are obtained under the assumptions that the multiplets, which contribute to C1, are split into magnetic substates with $m_s = -|S_t|, ..., +|S_t|$ and that only $|\Delta m_s| = 1$ transitions occur. The constant terms account for a small contamination of the sample with monomers (see below). The numerical fits of $I_{112}T$ and I_rT yielded $J = 94$ cm^{-1} and $J = 132$ cm^{-1}, respectively. As the first value is much closer to the result derived from the magnetic susceptibility analysis than the second one, we are tempted to assign the isotropic signal C1 to the highest quintet $|112\rangle$. A more complicated coupling scheme than that shown in Scheme I with different coupling constants J_{ij} would probably improve these fits. However, the quality of the data does not justify the increase in the number of parameters in the analysis.

The small contribution in $I_{C1}T$ of the $g = 2.10$ signal C1, remaining below 50 K in Figure 4A, accounts for only 2.2% of relative spin concentration. Because it obeys a Curie–Weiss law, we attribute it to an artifact of Cu(II) monomers, corresponding to the small $S = {}^1/_2$ impurity found also in the magnetic susceptibility measurement.

Magnetostructural Correlation. Although the Cu–N(Im) bond distance of 1.985 Å in the present compound is shorter than that of the previously reported trinuclear complex,[10] $[(C_9H_{21}N_3)_3Cu_3(Im)_3]^{3+}$, the coupling in the tetranuclear complex, $[(C_6H_{15}N_3)_4Cu_4(Im)_4]^{4+}$, is weaker than that in the trinuclear complex (Table IV). Thus the Cu–N(Im) bond distance seems to be less important in determining the magnitude of the exchange interaction than for example bond angles.

The interaction between the copper centers through the imidazolate bridging ligand can be explained in terms of a σ- and/or a π-exhange pathway. In general there is agreement[12,25,27] that the π-orbitals of the imidazolate ligand are not involved in the coupling. It has been stated that, since the magnetic orbitals are σ-antibonding for square planar and square pyramidal complexes, the relevant exchange pathway through the imidazolate bridge is of the σ-type. The imidazolate orbitals that are responsible for this sort of interaction are of the type sketched in Figure 6, and they are essentially parallel to the N–N′ (or C–C) direction.

Several studies have already been reported[12,13,15] in which structural data have been used to find correlations between structure and exchange coupling in imidazolate-bridged copper(II) complexes. In Table IV the structural parameters which appear to be responsible for the exchange coupling constant are listed for several structurally characterized imidazolate-bridged (which is not a part of a ligand) complexes. Different angles listed in the Table IV are defined in the following sketches:

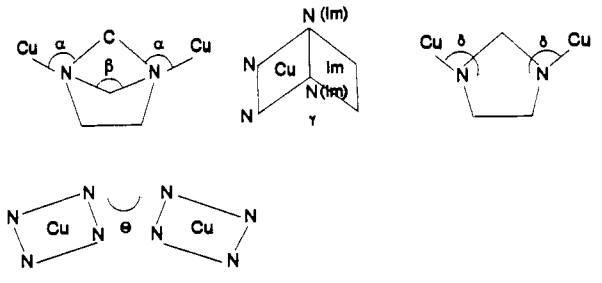

(26) Bencini, A.; Gatteschi, D. *Electron Paramagnetic Resonance of Exchange Coupled Systems*; Springer-Verlag: Berlin, 1990.

(27) Haddad, M. S.; Hendrickson, D. N. *Inorg. Chem.* **1978**, *17*, 2622.

Table IV. Exchange Coupling Constants and Structural Parameters for Imidazolate-Bridged Copper(II) Complexes

complex	J/cm^{-1}	α, deg	β, deg	γ, deg	δ, deg	θ, deg	ref
catena-$[Cu_3(Im)_2(ImH)_8(ClO_4)_4]$	117	130.6		70.0	162.9		23, 15
		129.8		60.0	160.9		
catena-$[Cu(Im)(ImH)_2Cl]$	84	135.3		90.0	169.4		24, 15
		128.5		90.0	168.8		
$[L'_3Cu_3(Im)_3](ClO_4)_3$	75	127.0	131.1	91.2	154.0	74.3	10, this work
		123.0	135.3	74.3	157.4	61.0	
		120.5		56.2	154.5	56.2	
						91.2	
$[L_4Cu_4(Im)_4](ClO_4)_4$	70	130.4	134.6	76.9	157.7	63.8	this work
		126.6	142.1	50.2	164.4		
		126.7		95.7	156.9		
				26.9	157.6		
$[Cu_4(Bpim)_2(Im)_2](NO_3)_4$	70	120.0		97.3		153	12
		128.0		100			
$[Cu_2(TMDT)_2(Im)[(ClO_4)_3$	52	129.0	143.0	91.8	161.9		12
		129.0		90.0	160.2		
$[Cu_2(Pip)_2(Im)](NO_3)_3$	54	121.0		95.0			12
		120.0		80.1			
		124.0		90.0			
		128.0		77.4			
$[Cu_2(Macro)(Im)](ClO_4)_3$	42	129.1		68.8	158.9		29
		134.4		79.1	166.3		
$[Cu_2(Schiff\ Base)(Im)](CF_3SO_3)_3$	38.6	128.9	128.0	93.4		45.2	17
		126.5	133.0	91.4			
			140.0				
$Na[Cu_2(Gly\text{-}Glyo)_2(Im)]$	38	124.5	135	5.8	157.5	5.9	16
		124.1		10.4	157.2		

[a] Im = imidazolate(1–), L = 1,4,7-triazacyclononane, L' = 1,4,7-trimethyl-1,4,7-triazacyclononane, Bpim = 4,5-bis[2-[[(2-pyridyl)ethyl]imino]-methyl]imidazolate, TMDT = *N,N,N',N'*-tetramethyldiethylenetriamine, Pip = 2-[2-[[(2-pyridyl)ethyl]imino]methyl]pyridine, Macro = a 30-membered macrocyclic ligand derived from 2,6-diacetylpyridine and 3,6-dioxaoctane-1,8-diamine, Gly-Glyo = glycylglycinate(2–), Schiff Base = macrocycle prepared from 2 molecules of 2,6-diacetylpyridine and 2 molecules of *m*-xylenediamine.

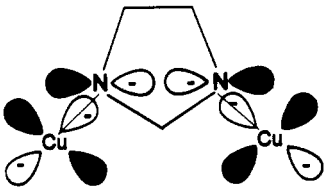

Figure 6. Schematic representation of the orbital orientations for the Cu–Im–Cu unit.

Comparison of the numerical data in Table IV shows that apparently there does not exist a simple magnetostructural correlation in these imidazolate-bridged Cu(II) complexes. At least it is obvious from the data that J values are independent of the angles, θ, between the two CuN_4 coordination planes, thus disfavoring the π-exchange path.

Data in Table IV show that the magnitude of J does not correlate strictly with the values of any of the single angles α, β, γ, or δ. However, on the basis of theoretical calculations,[27] it has been demonstrated that a maximum value of J is obtained when the Cu–N bonds are parallel to the imidazolate carbon–carbon bond, therefore favoring a σ-exchange pathway. An increase in α, β and δ angles should then produce a stronger coupling. Examination of Table IV shows that the same value of J for the tetranuclear complexes, $[L_4Cu_4(Im)_4]^{4+}$ and $[Cu_4(Bpim)_2(Im)_2]^{4+}$, cannot be strictly attributed to α and γ, probably, therefore, indicating that the σ superexchange pathways cannot be the only mechanism for exchange coupling in these compounds. A similar consideration holds also for the last two compounds of Table IV, exhibiting practically the same coupling constant, $J = 38\ cm^{-1}$. That a too strict dependence of the experimental coupling on structural parameters cannot be obtained has been pointed out[15] from extended Hückel calculations performed on model complexes $[Cu_2Cl_6(Im)]^{3-}$ and $[Cu_2(NH_2)_6(Im)]^{3-}$. It may be recalled that the effect of the angle δ between Cu–N(Im) and N–N(Im) vectors on J is related to the overlap of the inmidazolate orbitals and those of the second ligand in the coordination sphere of the metal, i.e. ligand–ligand interactions rather than metal–ligand interactions.

The strongest coupling[28] known to date for an imidazolate-bridged copper(II) complex is found to be $163\ cm^{-1}$ in a compound containing a chelating imidazolate ligand. The interaction between two copper ions in such a complex is much smaller than that between type III coppers in proteins which exhibit extremely strong antiparallel interactions. These observations suggest that the imidazolate-bridged dicopper(II) structure, Cu–Im–Cu, cannot be expected to be involved in proteins having type III coppers. Actually a recently refined crystal structure[31] of ascrobate oxidase clearly shows that a water-derived ligand, OH^- or O^{2-}, is the type III copper bridging ligand in this metalloprotein.

Acknowledgment. Partial financial support by the DFG is gratefully acknowledged. Special thanks are due to Prof. K. Wieghardt for his help and interest.

Supplementary Material Available: Listings of complete crystallographic data (Table IS), intraligand bond distances and angles (Tables SI and SII), hydrogen atom coordinates (Table SIII), and anisotropic thermal parameters (Table SIV) (6 pages). Ordering information is given on any current masthead page.

(28) Dewan, J. C.; Lippard, S. J. *Inorg. Chem.* **1980**, *19*, 2079.
(29) Drew, M. G. B.; McCann, M.; Nelson, S. M. *J. Chem. Soc., Dalton Trans.* **1981**, 1868.
(30) Trautwein, A. X.; Bill, E.; Bominaar, E. L.; Winkler, H. *Struct. Bonding* **1987**, *78*, 1.
(31) Messerschmidt, A.; Ladenstein, R.; Huber, R.; Bolognesi, M.; Avigliano, L.; Petruzelli, R.; Rossi, A.; Finazzi-Agró, A. *J. Mol. Biol.* **1992**, *224*, 179.